Research Square

Preprints are preliminary reports that have not undergone peer review.
They should not be considered conclusive, used to inform clinical practice,
or referenced by the media as validated information.

Thermo-poro-elastic stress induced aperture alteration of 3-D fractured geothermal reservoirs and its effect on geothermal energy production

Abhijit Chaudhuri

abhijit.chaudhuri@iitm.ac.in

Indian Institute of Technology Madras

Shradharghya Shankar Adhikary

Indian Institute of Technology Madras

Chandrasekhar Annavarapu

Indian Institute of Technology Madras

Research Article

Keywords: Geothermal energy, Three-dimensional fracture network, Fracture aperture, Fracture permeability, Fully coupled thermo-hydro-mechanical model

Posted Date: June 11th, 2026

DOI: https://doi.org/10.21203/rs.3.rs-9842072/v1

License: This work is licensed under a Creative Commons Attribution 4.0 International License.
Read Full License

Additional Declarations: No competing interests reported.

Thermo-poro-elastic stress induced aperture alteration of 3-D fractured geothermal reservoirs and its effect on geothermal energy production

Abhijit Chaudhuri[1*], Shradharghya Shankar Adhikary[1] and Chandrasekhar Annavarapu[2]

[1]Department of Applied Mechanics and Biomedical Engineering, Indian Institute of Technology Madras, , India, Chennai, 600 036, Tamil Nadu, India.
[2]Department of Civil Engineering, Indian Institute of Technology Madras, , India, Chennai, 600 036, Tamil Nadu, India.

*Corresponding author(s). E-mail(s): abhijit.chaudhuri@iitm.ac.in;
Contributing authors: shradhar1997@gmail.com; annavarapuc@iitm.ac.in;

Abstract

Many geothermal reservoirs are naturally or hydraulically fractured media. The thermo-poro-elastic stress that is induced within the reservoir due to the cooling of reservoir during heat extraction by water circulation, influences the opening and closing of fractures, and subsequently change the effective transmissvity of the reservoir. In the present study, we have developed a three-dimensional model of coupled flow, heat transfer, and deformation of fractured rock including the aperture alteration of 3D fracture networks. Three-dimensional fracture networks of randomly oriented rectangular fractures with different sizes and dip angles have been created using ADFNE Matlab code. We have represented the fracture as equivalent porous medium, enabling convenient modeling of fracture aperture evolution using FEHM, a highly resilient computational framework designed for coupled simulation of geothermic and geomechanics. We have observed that thermal contraction of rock reduces the compressive stress in many parts of the reservoir and even in the vicinity of the injection well, fractures are subjected to tensile stress. However, outside the fractured zone where the temperature change is negligible, stress become more compressive. After each time step the normal and shear stress and change in pore pressure at all nodes within the fracture are calculated and then these are used to determine local aperture using appropriate relations proposed in past literature. We have observed that the aperture growth due to tensile stress near injection well enhances the effective reservoir transmissivity, reduces injection pressure and most importantly cause faster temperature drawdown.

Keywords: Geothermal energy, Three-dimensional fracture network, Fracture aperture, Fracture permeability, Fully coupled thermo-hydro-mechanical model

- THM modeling of geothermal systems includes aperture alteration of 3D fracture networks
- Thermal contraction of rock causes tensile stress between wells and compressive stress in outer regions
- Aperture increase due to tensile stress near injection well can be more than 10 times

- THM simulation including aperture alteration predicts faster temperature drawdown.
- Increase of effective reservoir transmissivity reduces injection pressure

1 Introduction

Geothermal energy is a renewable energy source characterized by vast reserves (Soltani et al. 2021), minimal environmental pollution, and long-term sustainability (Ma et al. 2022). The abundance of deep, hot dry rock resources has driven rapid advancements in Enhanced Geothermal System (EGS) modeling and experimental research. However, developing a comprehensive multiphysics coupling model for dual porous media remains a significant challenge. In particular, modeling reservoir deformation resulting from the interplay of thermal, hydraulic, and mechanical processes is critical for geothermal heat extraction. A key parameter governing this process is fracture permeability, which controls fluid flow and heat transfer within the reservoir and evolves continuously due to changes in stress, temperature, and pore pressure.

Several studies have investigated the coupled thermal-hydro-mechanical (THM) processes governing heat extraction from geothermal reservoirs. Martinez et al. (2014) examined conductive and advective heat transfer within a saturated rock matrix and fracture system. Deo et al. (2014) explored how working fluid selection, fracture density distribution, and multilayer fracture configurations influence heat extraction from sandstone and granite geo-reservoirs. Sun et al. (2017) developed a discrete fracture network model to replicate THM interactions during geothermal heat extraction. Najari and Selvadurai (2014) studied the THM responses of granite rock under thermal fluctuations during heat extraction, though without accounting for changes in fluid and rock properties. Shaik et al. (2011) determined effective permeability tensors to simulate fluid flow within a two-dimensional geothermal reservoir model. Ghassemi and Zhou (2011) demonstrated that thermo-elastic effects dominate reservoir behavior over its production life, while poro-elastic phenomena are most significant during early stages; they further showed that cooling induces tensile stresses near injection zones, which diminish as pore pressure decreases over time. Gelet et al. (2012) simulated coupled THM processes in fractured high-temperature geo-reservoirs under local thermal non-equilibrium conditions, finding that solid contraction near the injection well induces tensile effective stress and increases fracture aperture. Liu et al. (2015) demonstrated that spatial variability in fracture aperture governs fracture permeability and highlighted the importance of accounting for fracture profiles in permeability modeling, using COMSOL Multiphysics. Doonechaly et al. (2016) investigated alterations in fracture permeability due to porosity, temperature, and elasticity effects as cold fluid circulates through a discrete fracture network. More recently, (Song et al. 2022; Zhang et al. 2023) proposed that natural fractures connected to longer hydraulic fractures enhance EGS performance and developed a THM-coupled model for EGS with multilateral wells. Zhang et al. (2023) further employed the extended finite element method to evaluate heat energy production under fully coupled THMC conditions using an embedded discrete fracture model. Zhao et al. (2023) developed a THM-coupled model to study permeability evolution during reservoir unloading in EGS.

While these studies have advanced the understanding of fracture aperture and permeability evolution during geothermal energy extraction, a critical gap remains: no study has simultaneously examined the coupled effects of normal stress, shear dilation, and fluid pressure on fracture permeability and their collective influence on heat transport within a three-dimensional, arbitrarily oriented fracture network. Addressing this gap is essential, as the nonlinear interdependence of fluid flow, heat transfer, stress, and

deformation – including both elastic and plastic responses and the pressure- and temperature-dependent behavior of rock properties – introduces complexities that cannot be captured by existing models. In the present study, a thermo-hydro-mechanical (THM) model is developed to analyze aperture variations arising from normal stress, shear dilation, and pore pressure changes, and their consequent effects on permeability and energy production. While the governing equations for heat transfer, momentum and mass balance are solved in a fully coupled manner, the aperture alteration relation is explicitly coupled with the framework to improve the nonlinear convergence behavior.

2 Mathematical and numerical modeling

This section gives an overview of the governing equations for the three-field thermo-hydro-mechanically coupled formulation with temperature, pressure and displacements as the field variables. The aperture alteration relationship, the model geometry and the boundary conditions used in the numerical simulations and the numerical modeling approach used in the study are also described here.

2.1 Governing equations

The general equations for advective and conductive heat transport in a 3-D porous reservoir is given as follows:

$$\frac{\partial}{\partial t}\left(\left(\rho c_P\right)_m T\right) + \mathbf{q}.\nabla H - \nabla.\left(\lambda \nabla T\right) = 0 \tag{1}$$

where T, H, c_p, ρ, λ, $\mathbf{q}$, ∇ are the temperature, enthalpy, specific heat, density, thermal conductivity, seepage flux, and differential operator. The heat capacity for the porous medium is defined as:

$$\left(\rho c_p\right)_m = \left(1-\phi\right)\left(\rho c_p\right)_{solid} + \phi\left(\rho c_p\right)_{fluid} \tag{2}$$

where ϕ is the porosity in a matrix.

The equation describing fluid flow within a permeable reservoir is characterized by Darcy equation:

$$\mathbf{q} = -\frac{k}{\mu}\left(\nabla p - \rho_f \mathbf{g}\right) \tag{3}$$

where k is the permeability and p is the pressure of the fluid within the porous rock medium. $\mathbf{g}$, μ, ρ_f are gravitational acceleration, the dynamic viscosity, and the density of water.

For modeling the deformation of fractured porous medium, the force balance equations are provided as follows,

$$\nabla \cdot \boldsymbol{\sigma} + \rho_b \mathbf{g} = 0 \tag{4}$$

where $\boldsymbol{\sigma}$ is the total stress tensor, ρ_b is the bulk density of the porous medium and $\mathbf{g}$ is the gravitational acceleration vector. In case of thermo-poro-elastic deformation, the following constitutive relationship holds

$$\boldsymbol{\sigma} = \boldsymbol{\sigma'} - \alpha_b p \mathbf{I}, \tag{5}$$

$$\boldsymbol{\sigma'} = 2\mu\boldsymbol{\epsilon} + \lambda\ \mathrm{tr}(\boldsymbol{\epsilon})\mathbf{I} - \beta K \Delta T \mathbf{I}, \tag{6}$$

$$\boldsymbol{\epsilon} = \frac{1}{2}\left(\nabla\mathbf{u} + \nabla^T\mathbf{u}\right), \tag{7}$$

where $\boldsymbol{\sigma'}$ is the effective stress tensor and $\boldsymbol{\epsilon}$ is the small strain tensor. α_b is Biot coefficient, β is thermal expansion coefficient, K is bulk modulus and $\mathbf{I}$ is the identity tensor, and λ and μ denote the Lamé's constants.

The mass balance equation accounting for fluid and rock compressibility:

$$\frac{1}{M}\frac{\partial p}{\partial t} + \alpha_b \frac{\partial \mathrm{tr}(\boldsymbol{\epsilon})}{\partial t} = \frac{1}{\rho_f}\nabla \cdot \left(\rho_f \frac{k}{\mu}\left(\nabla p - \rho_f \mathbf{g}\right)\right) \tag{8}$$

where M is the Biot modulus and all other symbols are as previously defined.

2.2 Aperture alteration

The constitutive relations for modeling the temporal and spatial evolution of stress-dependent aperture (b) under different stress states are discussed below.

2.2.1 Normal closure

The normal stress directly affects the alteration of fracture aperture. Previously proposed models that account for the coupling between stress and permeability in fractures have been demonstrated by (Barton and Choubey 1977; Bandis et al. 1983). These models effectively capture the behavior of fracture aperture when subjected to in situ stress, particularly in scenarios involving normal closure. The relation between local change in fracture aperture Δb_{normal} and normal compressive stress at the fracture plane σ'_n:

$$\Delta b_{normal} = \frac{9 b_{ini} \sigma'_n}{\sigma_{nc} + 10\sigma'_n} \tag{9}$$

where, b_{ini} is initial fracture aperture and σ_{nc} is the critical normal stress. It is expressed as, $\sigma_{nc} = -0.487 b_{ini} - 2.51$ (Gan and Elsworth 2016), where b_{ini} is in mm and σ_{nc} is in MPa (negative sign is for compression) .

2.2.2 Shear dilation

Fracture shear slip refers to the relative displacement that occurs between two fracture walls. Dilation is the variation in the aperture of fracture that occurs as a result of a shear slip. The increase in aperture b_{shear} caused by shear dilation can be computed as follows (Gan and Elsworth 2016):

$$\Delta b_{shear} = \frac{\tau - \tau_{sc}}{K_s} \tan(\phi_d) \tag{10}$$

where τ is the total shear stress along the fracture plane, ϕ_d is the dilation angle, K_s and initial joint shear stiffness and τ_{sc} is critical shear stress which is given as, $\tau_{sc} = -\sigma'_n \tan(\phi)$, where ϕ is the friction angle and negative sign is because the critical shear stress is related to compressive stress.

2.2.3 Fracture walls out of contact

When the pressure of the fluid surpasses the total normal stress σ_n applied to the fracture walls, it pushes the fracture walls apart and subsequently the fracture aperture further increases. This can also happen under tensile loading. The scenario where fracture walls are out of contact is particularly pronounced in fluid-filled fractures where the fluid pressure acts uniformly on both sides of the fracture (Crouch et al. 1983). Conversely, if the fluid pressure decreases or is lower than the confining stress (the contrast between the pore pressure and applied stress), the fracture walls may close, reducing the aperture (Gan and Elsworth 2016). Due to excess fluid pressure, the increase of aperture, Δb_{open}, is calculated as follows.

$$\Delta b_{open} = \frac{p_f - p_{f0}}{10 \times \frac{7\pi}{24}\frac{G}{r}} \tag{11}$$

where $p_{f0} = \sigma_n$, r is half-length of a circular fracture.

2.2.4 Overall effect

When the effective normal compressive stress is positive and the fracture walls are in contact due to the presence of nails and asperities. In such cases, the fracture aperture alteration is determined as the sum of Δb_{normal} and Δb_{shear} which are calculated using Eqs. 9 and 10, respectively. The expression of the resulting aperture is given as,

$$b = b_{ini} + \frac{9 b_{ini}\sigma'_n}{\sigma_{nc} + 10\sigma'_n} + \frac{\tau - \tau_{sc}}{K_s}\tan(\phi_d) \tag{12}$$

When the fluid pressure inside the fracture exceeds the total normal stress due to confinement, the resulting aperture is given as (Gan and Elsworth 2016),

$$b = b_{ini} + \frac{9 b_{ini}\sigma'_n}{\sigma_{nc} + 10\sigma'_n} + \frac{\tau - \tau_{sc}}{K_s}\tan(\phi_d) + \frac{p_f - p_{f0}}{10 \times \frac{7\pi}{24}\frac{G}{r}} \tag{13}$$

For fractures, the permeability is calculated as

$$k = \frac{b^3}{12 b_p} \tag{14}$$

where, b_p is the thickness of the equivalent porous media.

2.3 Calculation of normal and shear stress along fracture plane

Note that σ_n and τ are defined in the coordinate plane of the fracture which may be different from the global coordinate system and therefore one must compute them through appropriate coordinate transformations. An illustration of this procedure is described in this subsection. For any finite element within a given fracture, the total stress tensor, $\boldsymbol{\sigma}$, is obtained from thermo-poro-elastic simulation using FEHM. To derive the normal and shear stress components along the fracture the stress tensor, $\boldsymbol{\sigma_F}$, is calculated as,

$$\boldsymbol{\sigma_F} = \mathbf{e}^{\intercal} \cdot \boldsymbol{\sigma} \cdot \mathbf{e}, \tag{15}$$

where, $\mathbf{e} = \begin{bmatrix}\mathbf{n} & \mathbf{s_1} & \mathbf{s_2}\end{bmatrix}$. It is the coordinate transformation matrix for the arbitrarily inclined fracture. The procedure to obtain $\mathbf{e}$ for ABCD fracture as shown in Fig. 1 is illustrated below. The rectangle ABCD indicates the mid-plane of the fracture. The unit vector ($\mathbf{n}$) and two orthogonal tangential unit vectors ($\mathbf{s_1}$ and $\mathbf{s_2}$) along the fracture plane are shown in the Fig. 1. The methods to calculate the components of $\mathbf{e}$ are given below.

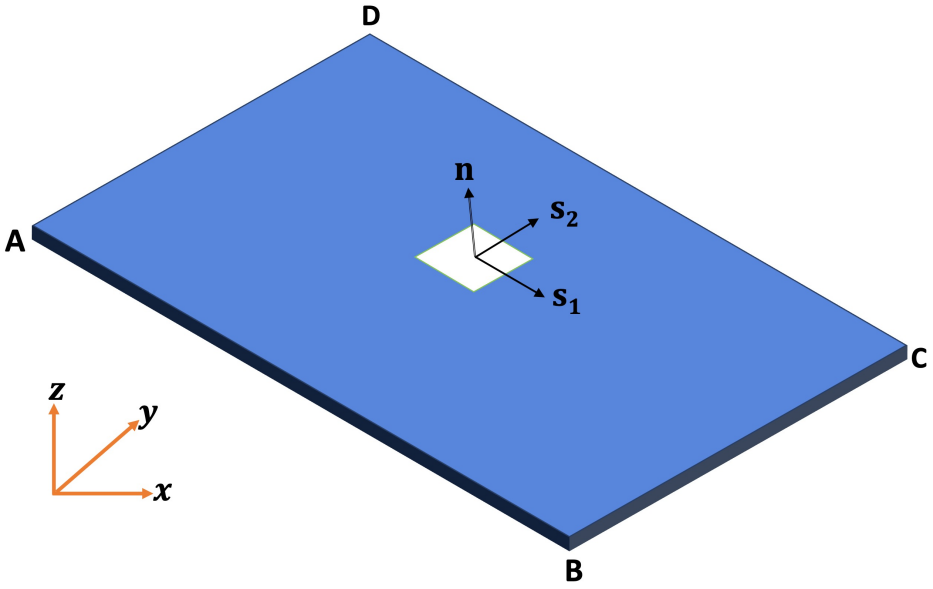


Fig. 1 Plane shows the unit normal vector and two other orthogonal tangential vectors along the plane.

$$\mathbf{a_1} = \begin{bmatrix} x_A - x_B & y_A - y_B & z_A - z_B \end{bmatrix}^{\mathsf{T}};$$

$$\mathbf{a_2} = \begin{bmatrix} x_C - x_B & y_C - y_B & z_C - z_B \end{bmatrix}^{\mathsf{T}};$$

$$\mathbf{b_1} = \mathbf{a_1} \times \mathbf{a_2};$$

$$\mathbf{b_2} = \mathbf{a_1} \times \mathbf{b_1};$$

$$\mathbf{n} = \mathbf{b_1}/|\mathbf{b_1}|;$$

$$\mathbf{s_1} = \mathbf{a_1}/|\mathbf{a_1}|;$$

$$\mathbf{s_2} = \mathbf{b_2}/|\mathbf{b_2}|;$$

The local values of effective normal compressive stress and resultant shear stress along the fracture plane are obtained as

$$\sigma_n' = \sigma_{F1,1} + \alpha_b p \tag{16}$$

$$\tau = \sqrt{\sigma_{F1,2}^2 + \sigma_{F1,3}^2} \tag{17}$$

2.4 Model geometry and boundary conditions

The computational domain of a three-dimensional reservoir containing arbitrarily oriented fracture networks of 30 and 50 fractures is shown in Fig. 2. Figure 3 shows two networks of fractures considered in this study. These interconnected fracture networks connect an injection and a production well. The dimensions for the idealized reservoir are specified as 1000 meters in the x-direction, 1000 meters in the y-direction, and 300 meters in the z-direction, as depicted in Fig. 2. The computational domain is

1 km below the ground surface, the fractured domain, measuring 500 meters in the x-direction, 500 meters in the y-direction, and 200 meters in the z-direction, is centrally positioned within the larger computational domain as shown in Fig. 2 to minimize the effect of boundary conditions on heat transfer in the region of interest. Injection and production wells have been strategically located at the farthest points within the fractured zone.

In the current study, the temperature of injection is set at 45 °C, while the initial reservoir temperature is specified as 85 °C. The boundary conditions along different faces are listed below.

- Vertical side boundaries (ABCD, BFGC, FEHG and EADH): $\mathbf{q}_\alpha \cdot \mathbf{n} = 0$, $T = T_{res}$, and $\sigma_{n,t} = \sigma_{n,t_{insitu}}$.
- Top boundary (ABFE): $p = p_{top} = 10$ MPa, $T = T_{res}$, and and $\sigma_{n,t} = \sigma_{n,t_{insitu}}$.
- Bottom boundary (DCGH): $\mathbf{q}_\alpha \cdot \mathbf{n} = 0$, $T = T_{res}$, and $\mathbf{u} = \mathbf{0}$.
- Injection zone (red circle): $\dot{m}_{inj} = 25$ kg/s, and $T = T_{inj}$.
- Production zone (blue circle): $p = p_{pro} = 9$ MPa.

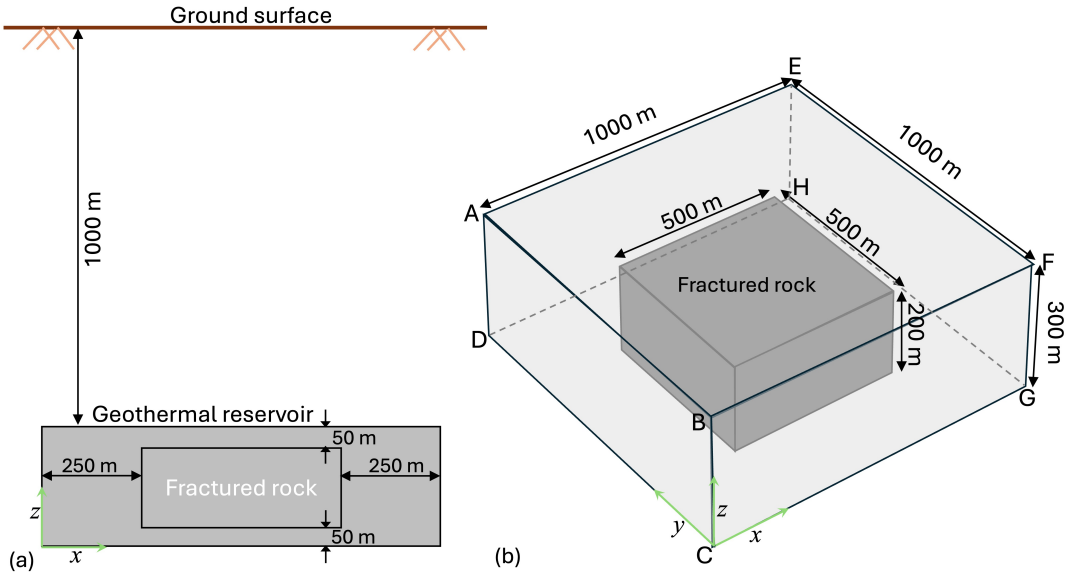


Fig. 2 Schematic diagram to show the depth of the geothermal reservoir below the ground surface and computational domain for the simulating coupled flow, heat transfer and geomechanics.

2.5 Numerical modeling approach

We model fractures as equivalent thin porous layers, and a nonlinear joint model as described in Section 2.2 is incorporated into FEHM. When simulating aperture alterations in fractures or rock joints, we employed a simplified hyperbolic model. Additionally, we introduced a linear relationship between the increment in fracture aperture resulting from shear dilation and normal opening displacement and the increase in fluid pressure consistent with Gan and Elsworth (2016). Furthermore, we derived a relationship for the non-linear stress-strain behaviour of the equivalent porous layer to ascertain permeability alterations. In our study, we also considered the mechanical properties of the reservoir rock to assess their influence on changes in aperture and the functioning of heat extraction when injecting cold

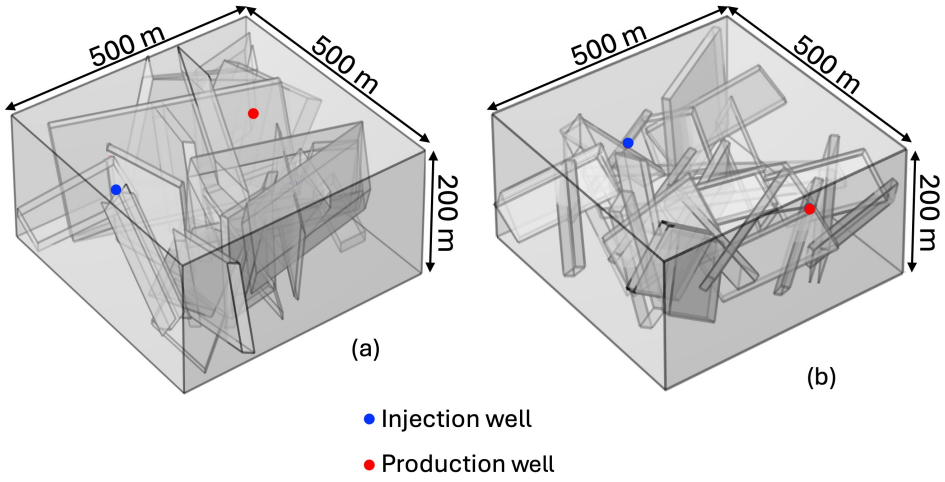


Fig. 3 Representative fracture network with (a) 30 fractures, and (b) 50 fractures. The bottom holes of injection well and production well are indicated by blue and red dots, respectively.

water into the fracture.

The coupled THM simulations, including the aperture and fracture permeability evolution, have been performed sequentially. For each time step, all of the governing equations (Eqs. 2 - 8) are solved, considering implicit coupling using FEHM. At the end of each time step, the values of normal and shear stress components for all nodes lying within different fractures are computed using the procedure outlined in Subsection 2.3. These nodal values of σ_n', τ and p_f are then used to determine the new aperture and permeability of the fracture nodes using the equations provided in Subsection 2.2. Thus, fracture permeability evolution is explicitly coupled with THM simulation.

A non-uniform yet structured computational mesh was employed to achieve a solution of efficient and precise for the coupled THM problem shown in the Figure 4. In COMSOL Multiphysics 6.0, an extra-fine physically controlled hexahedral meshing technique was employed to generate meshes for fractured reservoirs with different fracture networks. The minimum element size was set to 0.2 m, while the maximum element size was set to 20 m. A maximum element growth rate of 1.3 was utilized, along with a curvature factor value of 0.2. In the case of the fractured zone, the grid dimensions in the z direction are consistently uniform as $\Delta z = 20$ m, while in the x and y directions, they are also uniform $\Delta x = \Delta y = 10$m. However, outside the fracture zone, the grid dimensions remain uniform in the z direction $\Delta z = 20$m but vary in the x and y directions. The grid size is finer near the fractured zone and coarser as one moves away from the fractured zone. Specifically, the grid size in the x and y directions near the fractured zone is given as $\Delta x = \Delta y = 10$ m, while at the corner of the reservoir, the grid size is given as $\Delta x = \Delta y = 20$ m. The total number of mesh vertices is 99216.

The stress within the fractured zone, variations in fracture permeability and aperture values are all influenced by key factors. These factors include permeability, density, mobility, specific heat capacity, Young's modulus, and Biot's coefficient of the matrix and fractured zone. The specific values and constants for these parameters utilized in this study are detailed in the accompanying Table 1.

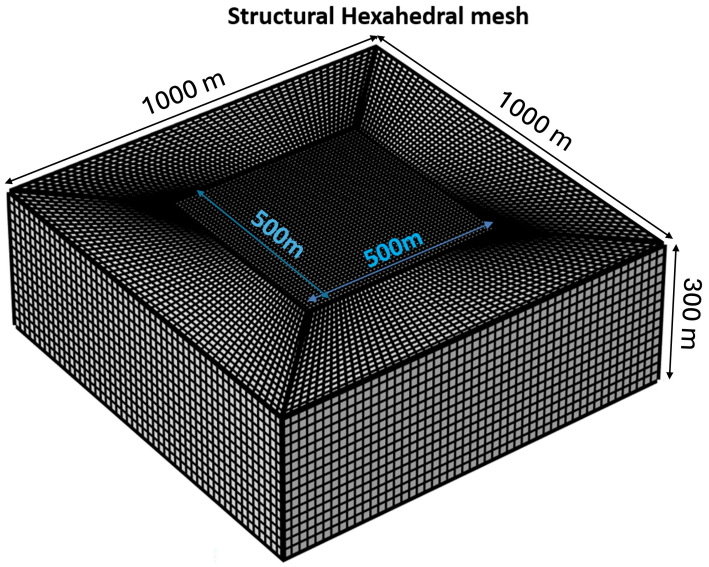


Fig. 4 Three-dimensional Structural Hexahedral mesh using COMSOL Multiphysics®6.0.

Table 1 Numerical modeling parameter used in the study.

Parameters	Rock Matrix	Equivalent permeable porous medium (Fracture)
Permeability	$k = 2 \times 10^{-20}$ m^2	Permeability calculated from fracture aperture
Porosity	$\phi = 0.1$	Porosity calculated from fracture aperture
Thermal conductivity	$\lambda = 2.5$ W/m/K	$\lambda = 2.5$ W/m/K
Specific heat capacity	$c_p = 1000$ J/kg/K	$c_p = 1000$ J/kg/K
Rock density	$\rho = 2500$ kg/m^3	$\rho = 2500$ kg/m^3
Biot's coefficient	$\alpha_b = 0.95$	$\alpha_b = 0.95$
Young's modulus	$E = 40$ GPa	$E = 1.6$ GPa
Poisson's ratio	$\nu = 0.3$	$\nu = 0.005$

3 Results and discussion

It is hypothesized that during high-pressure injection of cold water into a hot reservoir, the cooling effect and elevated pore pressure near the injection zone cause fracture apertures to expand and permeability to increase. This enhances fluid flow through fractures directly connecting the injection and production wells. Beyond the cooling zone, however, aperture decreases, confining flow to a smaller region of the fracture network and accelerating temperature drawdown at the production well. While these effects have been demonstrated in principle through THM modeling of simpler geothermal systems with a single horizontal fracture connecting the wells Pandey et al. (2017), their behavior within more complex, arbitrarily oriented fracture networks remains undemonstrated. The numerical examples in this section address this gap by illustrating these effects and quantifying the influence of aperture alteration across two different fracture networks on energy production.

Coupled thermo-hydro-mechanical (THM) and thermo-hydro (TH) simulations were performed for two fracture networks containing 30 and 50 fractures (Fig. 3). The TH-THM comparison isolates the effect of stress-dependent fracture aperture evolution on temperature drawdown, energy production rate, and injection pressure. Comparing TH results between the two networks, the 30-fracture network exhibits faster production temperature decline and higher injection pressure than the 50-fracture network (Fig. 5a,c). The higher injection pressure required by the 30-fracture network reflects lower fracture

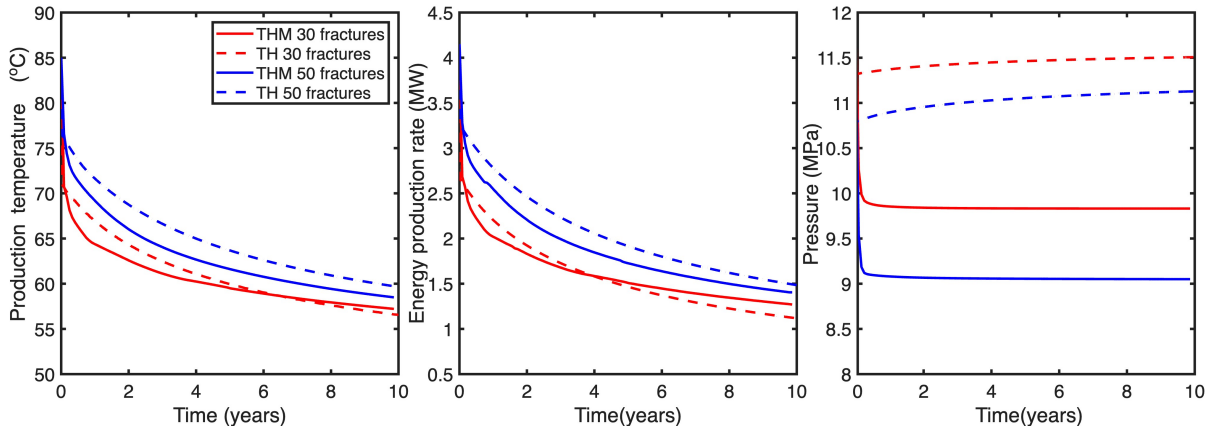


Fig. 5 Comparison of (a) production temperature, (b) energy production rate, and (c) injection pressure for 30, and 50 fractures to evaluate the impact of aperture changes by comparing the temporal variations of THM coupling (solid line) and TH coupling (dashed line).

connectivity, reduced heat transfer from the reservoir, and consequently faster temperature drawdown – consistent with findings reported by Adhikary et al. (2026).

When mechanical coupling is included, simulations accounting for thermo-poro-elastic fracture aperture evolution predict a more rapid decline in production temperature (Fig. 5a) and energy production rate (Fig. 5b) compared to TH-only simulations. This is because aperture expansion near the injection well preferentially channels flow along connected fractures, accelerating thermal breakthrough. For the 50-fracture network, THM and TH energy production rates converge over time, suggesting that greater fracture connectivity distributes the mechanical effects more broadly. In contrast, for the 30-fracture network, the THM simulation yields a slightly higher energy production rate after approximately 4 years, indicating that stress-driven permeability enhancement along the more limited fracture pathways sustains production more effectively at later times. Regarding injection pressure, THM simulations show an initial decrease of approximately 1 MPa shortly after extraction begins, while TH simulations show a gradual increase (Fig. 5c). This divergence confirms that aperture dilation driven by high injection pressure reduces flow resistance near the injection well, an effect absent in TH-only models.

The spatial and temporal evolution of temperature, effective stress, and permeability for the 30-fracture network are shown in Figs. 6 and 7. At the mid-plane ($z = 150$ m), temperature drops progressively over 10 years (Fig. 6, row 1), with cooling advancing more rapidly along fractures due to convective heat transfer and more gradually through the rock matrix via conduction. Rock contraction induced by cooling generates tensile stress within the fractured zone. The effective horizontal stress σ'_{xx} shifts substantially from its initial compressive value of -7.635 MPa, becoming predominantly tensile along fractures – exceeding +10 MPa near the injection well – while growing more compressive (below -10 MPa) in the unfractured rock above and below the fractured zone (Fig. 6, row 2). The vertical effective stress σ'_{zz}, initially -17.825 MPa, also increases but remains largely compressive except near the injection well, while the rock outside the fractured zone reaches values below -25 MPa (Fig. 6, row 3). Where the effective normal stress σ'_n becomes tensile, fractures open and aperture increase (Δb_{open}) dominates, driving permeability from its initial value of 5×10^{-12} m^2 to nearly 10^{-8} m^2 in the most strongly cooled

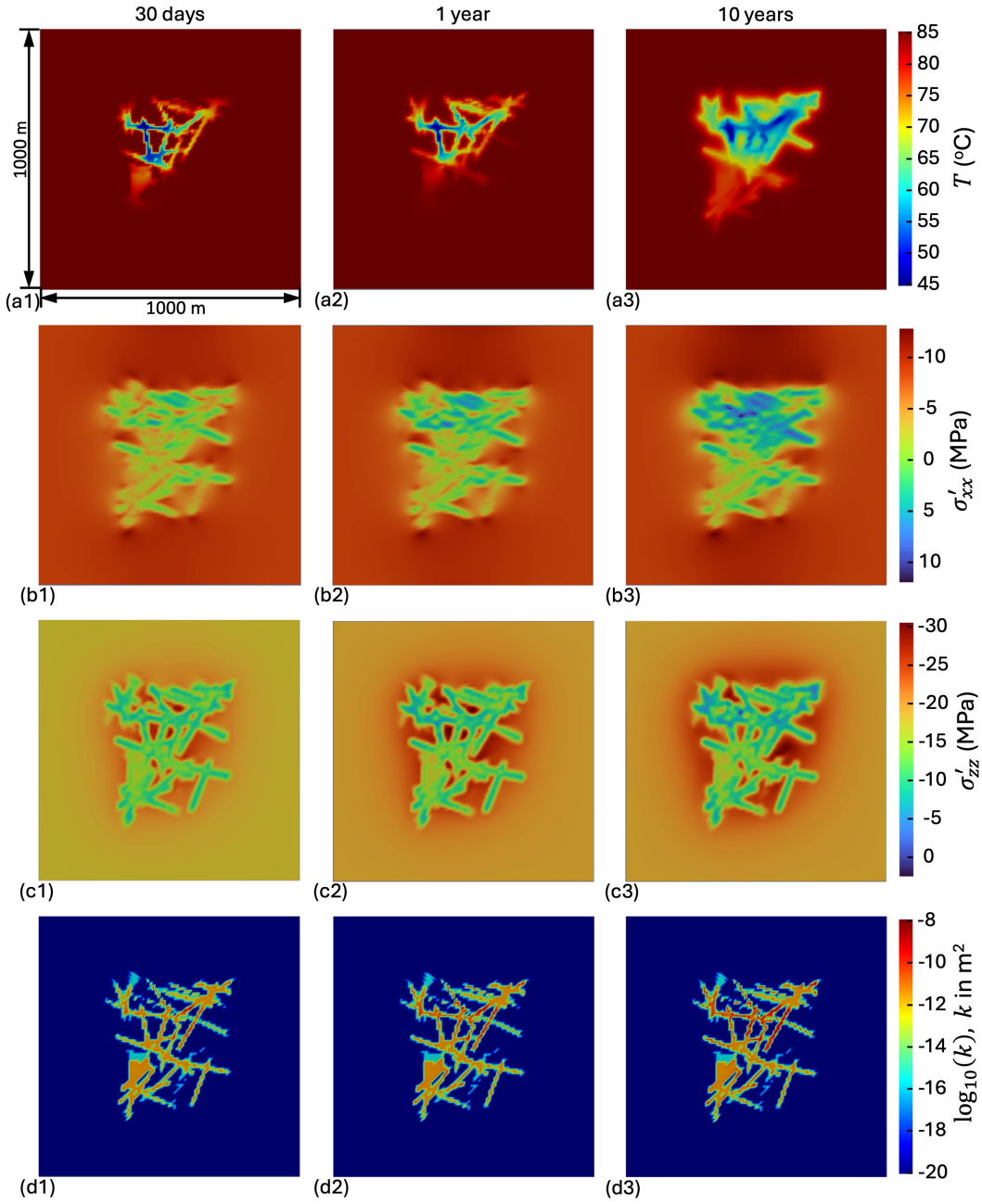


Fig. 6 Evolution of (a) temperature, (b, c) stresses in x and z directions and consequently (d) fracture permeability are shown by plotting the contours at $z = 150$ m after different times (a1,b1,c1,d1) 30 days, (a2,b2,c2,d2) 1 year, and (a3,b3,c3,d3) 10 years for 30 fracture networks.

regions. Permeability decreases in fractures subject to increased compression (Fig. 6, row 4).

Comparing across depth planes (Fig. 7), the greatest cooling and permeability enhancement occur at $z = 100$ m, where the injection well is located. The differing fracture counts, orientations, and temperature drops at each plane produce distinct effective stress fields, resulting in spatially heterogeneous permeability distributions across the reservoir depth.

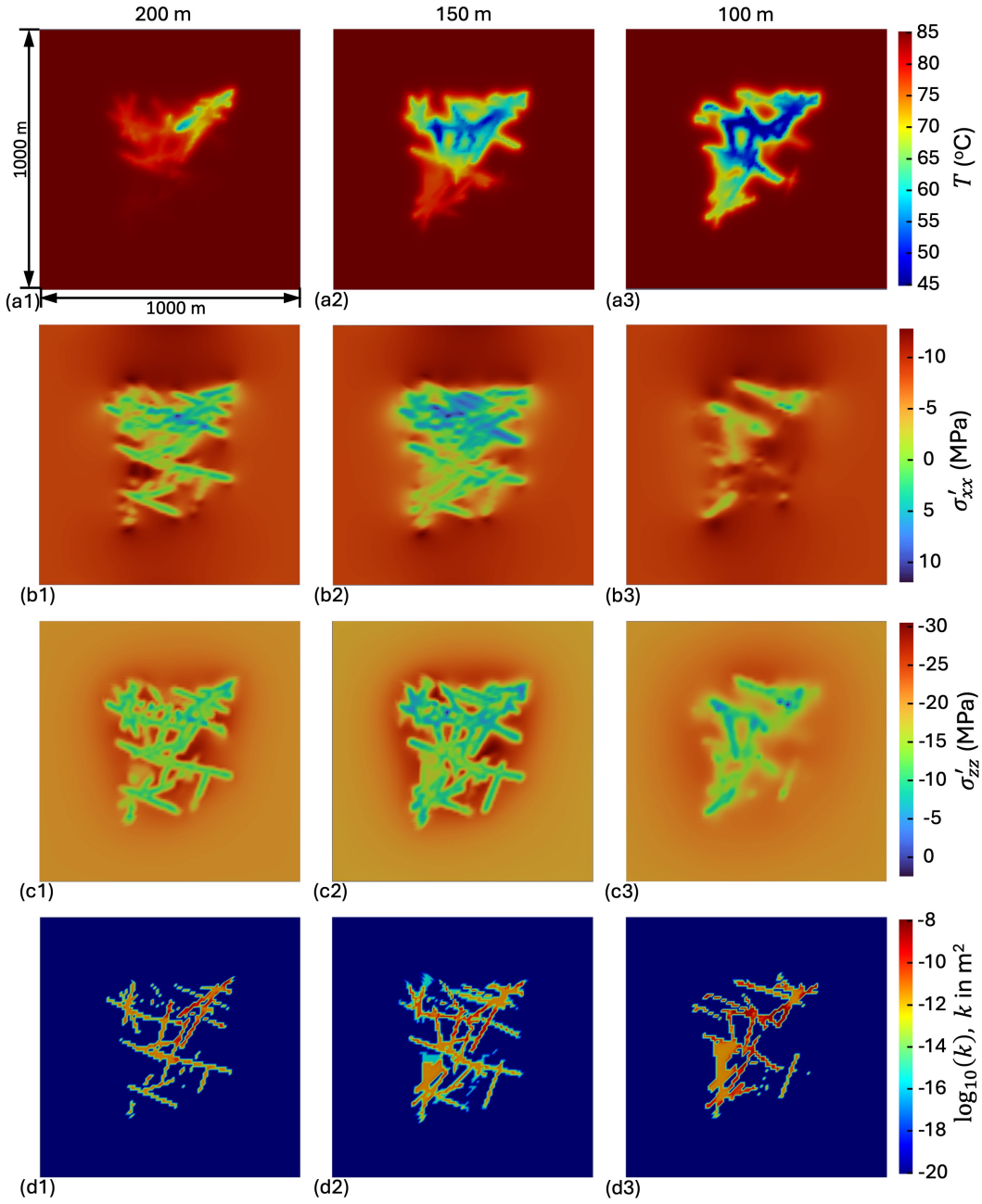


Fig. 7 Spatial variation of (a) temperature, (b, c) stresses in x and z directions and consequently (d) fracture permeability are shown by plotting the contours 10 years at (a1,b1,c1,d1) $z = 200$ m, (a2,b2,c2,d2) $z = 150$ m, and (a3,b3,c3,d3) $z = 100$ m for 30 fracture networks.

Finally, the vertical displacement field (Fig. 8) reflects the competing mechanical influences over time. Early in the simulation, high injection pressure drives upward displacement ($u_z > 0$). As extraction continues, progressive reservoir cooling and contraction reverse this trend, producing net downward displacement at later times. This mechanical response has direct implications for reservoir integrity and should be accounted for in long-term EGS operational planning.

Taken together, these results confirm the opening hypothesis: cold-water injection expands apertures and enhances permeability near the injection zone, accelerating thermal breakthrough, while aperture

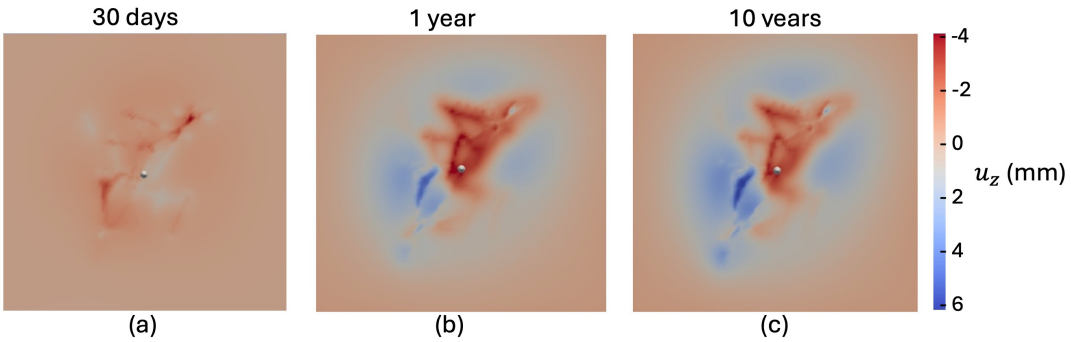


Fig. 8 Vertical displacement field(m) for 30 fractures over various time intervals shown in (a) 30 days, (b) 1 year & (c) 10 years.

reduction outside the cooling zone confines flow and further hastens temperature drawdown. The degree to which these coupled effects influence energy production depends critically on fracture network connectivity – with sparser networks amplifying stress-driven permeability changes and denser networks distributing them more uniformly across the reservoir.

4 Conclusions

In this study, a THM coupled model is developed to examine how the alteration of fracture aperture , due to thermo-poro-elastic deformation, influences the geothermal energy production and injectivity of geothermal reservoirs containing different fracture networks. A comprehensive relation is incorporated into FEHM, a software used to solve flow, heat transfer, and geomechanics implicitly, to determine the value of aperture based on the local values of normal and shear stress at the fracture, as well as fluid pressure in the fracture. However, coupling between THM simulation and the aperture alteration is managed explicitly. The important and novel findings based on the coupled simulations are highlighted below.

The contraction of rock due to cold water injection and continuous water circulation for geothermal energy extraction causes a significant decrease in compressive stress in the fractured zone and an increase in compressive stress mainly outside the fractured zone. In some parts of the fracture network, the effective normal stress in horizontal direction become tensile. In those locations, the fluid pressure pushes the fracture walls and aperture increases nearly by 10 times. The simulation results also show decrease in aperture of fractures which are away from the wells and subjected to higher compressive stress. Such spatial variation of aperture over time causes preferential flow and flow confinement which in turn reduces the heat extraction rate.

In the comparison of results based on the TH and THM models, we have found for both fracture networks that the alteration in permeability due to changes in fracture aperture causes a faster temperature drawdown and lower energy extraction rate. The increase in effective reservoir transmissivity also results in approximately 1 MPa decrease in injection pressure in the present scenarios. The alteration of stress state of the reservoir also leads both upward and downward vertical displacement at the top of the domain. Even though, the displacement is small in the present case, the deformation at the ground level can be critical depending on the duration of geothermal operation, temperature drawdown, mechanical and thermal properties of the reservoir rock, characteristics of the fracture network.

Appendix

Greek letters

α	Fluid phase
α_b	Biot's coefficient
β	Component
λ	Effective thermal conductivity (W/m/K)
μ	Dynamic viscosity (Pa.s)
ν	Poisson's ratio
ϕ	Porosity
ϕ_d	Dilation angle (°)
ρ	Density (kg/m^3)
σ	Normal stress (MPa)
σ_{insitu}	In situ stress (MPa)
τ	Shear stress (MPa)

Subscript/Superscript

inj	Injection zone
pro	Production zone
$insitu$	Insitu stress

Variables

g	Gravitational constant (m^2/s)
h	Injection well depth from the reservoir top (m)
k	Permeability (m^2)
m	Mass (kg)
q	Darcy flux ($m^3/(m^2.s)$)
t	Time (s)
x	Space coordinate (m)
y	Space coordinate (m)
z	Space coordinate (m)
c_p	Specific heat capacity (J/kg/°C)
h	Enthalpy (J)
m	Mass (Kg)
T	Temperature (°C)
b	Fracture aperture (m)
b_p	Thickness of the porous medium (m)
G	Shear modulas (GPa)
K_s	Initial joint shear stiffness (MPa)
p_f	Pore pressure(MPa)
p_{fo}	Total stress (MPa)

Acknowledgments

The authors are very thankful to IIT Madras for providing the computational facility of PG Senapathy Computer Center. This research work is a part of the M.S. thesis by Shradharghya Shankar Adhikary at IIT Madras, funded by MHRD, Government of India.

Data availability statement

The datasets generated during and/or analyzed during the current study are available from the corresponding author on reasonable request.

Competing Interest declaration

On behalf of all authors, the corresponding author states that there is no conflict of interest.

Compliance with Ethical Standards

This research presents an accurate account of the work performed, all data presented are accurate and methodologies detailed enough to permit others to replicate the work. This manuscript represents entirely original works. This material has not been published in whole or in part elsewhere. The manuscript is currently not being considered for publication in another journal.

Funding Declaration

There was no project funding for this study. However, we have acknowledged the supports from IIT Madras and MHRD, Government of India.

Ethical approval

The manuscript does not contain any data of clinical trial. The results and discussion are based on mathematical modeling and numerical simulations.

Consent to participate

Not applicable

Consent to publish

Not applicable

Author contributions

Conceptualization: [Abhijit Chaudhuri], [Shradharghya Shankar Adhikary], [Chandrasekhar Annavarapu];
Methodology: [Shradharghya Shankar Adhikary], [Abhijit Chaudhuri], [Chandrasekhar Annavarapu];
Formal analysis and investigation: [Shradharghya Shankar Adhikary], [Abhijit Chaudhuri];
Writing - original draft preparation: [Shradharghya Shankar Adhikary];
Writing - review and editing: [Abhijit Chaudhuri], [Chandrasekhar Annavarapu];

Funding acquisition: [Abhijit Chaudhuri];
Resources: [Abhijit Chaudhuri];
Supervision: [Abhijit Chaudhuri]

References

Adhikary, S.S., Chaudhuri, A., Annavarapu, C.: Numerical study of energy production from fractured rock hydrothermal reservoirs using co as the working fluid. Environmental Earth Sciences **85**(2), 47 (2026)

Barton, N., Choubey, V.: The shear strength of rock joints in theory and practice. Rock mechanics **10**, 1–54 (1977)

Bandis, S., Lumsden, A., Barton, N.: Fundamentals of rock joint deformation. In: International Journal of Rock Mechanics and Mining Sciences & Geomechanics Abstracts, vol. 20, pp. 249–268 (1983). Elsevier

Crouch, S.L., Starfield, A.M., Rizzo, F.: Boundary element methods in solid mechanics (1983)

Doonechaly, N.G., Azim, R.R.A., Rahman, S.S.: A study of permeability changes due to cold fluid circulation in fractured geothermal reservoirs. Groundwater **54**, 325–335 (2016) https://doi.org/10.1111/gwat.12365

Deo, M., Roehner, R., Allis, R., Moore, J.: Modeling of geothermal energy production from stratigraphic reservoirs in the great basin. Geothermics **51**, 38–45 (2014) https://doi.org/10.1016/j.geothermics.2013.10.011

Gan, Q., Elsworth, D.: A continuum model for coupled stress and fluid flow in discrete fracture networks. Geomechanics and Geophysics for Geo-Energy and Geo-Resources **2**(1), 43–61 (2016) https://doi.org/10.1007/s40948-015-0020-0

Gelet, R., Loret, B., Khalili, N.: A thermo-hydro-mechanical coupled model in local thermal non-equilibrium for fractured hdr reservoir with double porosity. Journal of Geophysical Research: Solid Earth **117**, 1–23 (2012) https://doi.org/10.1029/2012JB009161

Ghassemi, A., Zhou, X.: A three-dimensional thermo-poroelastic model for fracture response to injection/extraction in enhanced geothermal systems. Geothermics **40**, 39–49 (2011) https://doi.org/10.1016/j.geothermics.2010.12.001

Liu, R., Jiang, Y., Li, B., Wang, X.: A fractal model for characterizing fluid flow in fractured rock masses based on randomly distributed rock fracture networks. Computers and Geotechnics **65**, 45–55 (2015)

Ma, F., Liu, G., Zhao, Z., Xu, H., Wang, G.: Coupled thermo-hydro-mechanical modeling on the rongcheng geothermal field, china. Rock Mechanics and Rock Engineering **55**(8), 5209–5233 (2022)

Martinez, A.R., Roubinet, D., Tartakovsky, D.: Analytical models of heat conduction in fractured rocks. Journal of Geophysical Research: Solid Earth **119**(1), 83–98 (2014)

Najari, M., Selvadurai, A.P.S.: Thermo-hydro-mechanical response of granite to temperature changes. Environmental Earth Sciences **72**, 189–198 (2014) https://doi.org/10.1007/s12665-013-2945-3

Pandey, S., Chaudhuri, A., Kelkar, S.: A coupled thermo-hydro-mechanical modeling of fracture aperture alteration and reservoir deformation during heat extraction from a geothermal reservoir. Geothermics **65**, 17–31 (2017)

Soltani, M., Kashkooli, F.M., Souri, M., Rafiei, B., Jabarifar, M., Gharali, K., Nathwani, J.S.: Environmental, economic, and social impacts of geothermal energy systems. Renewable and Sustainable Energy Reviews **140**, 110750 (2021)

Shaik, A.R., Rahman, S.S., Tran, N.H., Tran, T.: Numerical simulation of fluid-rock coupling heat transfer in naturally fractured geothermal system. Applied thermal engineering **31**(10), 1600–1606 (2011)

Song, G., Song, X., Xu, F., Li, G., Shi, Y., Ji, J.: Contributions of thermo-poroelastic and chemical effects to the production of enhanced geothermal system based on thermo-hydro-mechanical-chemical modeling. Journal of Cleaner Production **377**, 134471 (2022)

Sun, Z.X., Zhang, X., Xu, Y., Yao, J., Wang, H., Lv, S., Sun, Z., Huang, Y., Cai, M., Huang, X.: Numerical simulation of the heat extraction in egs with thermal-hydraulic-mechanical coupling method based on discrete fractures model. Energy **120**, 20–33 (2017) https://doi.org/10.1016/j.energy.2016.10.046

Zhang, W., Han, D., Wang, B., Chen, Y., Jiao, K., Gong, L., Yu, B.: Thermal-hydraulic-mechanical-chemical modeling and simulation of an enhanced geothermal system based on the framework of extended finite element methods-embedded discrete fracture model. Journal of Cleaner Production **415**, 137630 (2023)

Zhao, P., Liu, J., Elsworth, D.: Numerical study on a multifracture enhanced geothermal system considering matrix permeability enhancement induced by thermal unloading. Renewable Energy **203**, 33–44 (2023)